



Experimental and DFT study of the degradation of 4-chlorophenol on hierarchical micro-/nanostructured oxide films

Victoire-Marie Guérin^a, Radek Zouzelka^{b,c}, Hana Bibova-Lipsova^{b,d}, Jaromir Jirkovsky^b, Jiri Rathousky^{b,*}, Thierry Pauporté^a

^a Institut de Recherche de Chimie Paris, CNRS – Chimie ParisTech- CNRS-PSL Research University, UMR8247, 11 rue Pierre et Marie Curie, 75005 Paris, France

^b Institute of Physical Chemistry, v.i.i., Academy of Sciences of the Czech Republic, Dolejskova 3, 18223 Prague 8, Czech Republic

^c Department of Physical Chemistry, Institute of Chemical Technology Prague, Technicka 5, 16628 Prague, Czech Republic

^d Institute of Hydrogeology, Engineering Geology and Applied Geophysics, Charles University in Prague, Albertov 3, 12800 Prague, Czech Republic

ARTICLE INFO

Article history:

Received 16 October 2014

Received in revised form

19 December 2014

Accepted 23 December 2014

Available online 27 December 2014

Keywords:

ZnO hierarchical nanostructures

Electrochemical deposition

Photocatalysis

4-Chlorophenol degradation

DFT modeling

ABSTRACT

Hierarchical ZnO nanoporous/nanowire architectures immobilized on a substrate were prepared by a facile two-step electrochemical technique. The layer optical properties have been characterized by absorption spectroscopy and photoluminescence measurements. The structures strongly absorbed UV light and had a high structural quality. The porosity of the hierarchical layers could be tuned by changing the duration of the second growth step. The photocatalytic activity of ZnO films was higher than that of arrayed ZnO nanowire layers and mesoporous ZnO films. The photocatalytic activity for 4-chlorophenol degradation could be enhanced by developing hierarchical structures with a high percentage exposure of polar (0001) facets, high specific surface area and good accessibility of the pollutant to the oxide surface. The modeling by density functional theory (DFT) of the degradation of 4-chlorophenol molecules by OH radicals lead to several important results, namely that the hydroxylation of the aromatic ring and its opening can occur in parallel releasing hydroperoxyl radical and hydroxyl radical, respectively. The restored OH radical can either further oxidize the primary ring opening product or attack another molecule of 4-chlorophenol. These computational results are in good agreement with the photocatalytic degradation observations made using both ZnO and TiO₂ photocatalysts.

© 2014 Elsevier B.V. All rights reserved.

1. Introduction

In recent years considerable attention has been devoted to the preparation of hierarchical structures of different materials. Zinc oxide-based micro-/nanoscale structures have attracted a considerable attention owing to their unique optical, electronic and physico-chemical surface properties as well as their reactivity [1,2]. ZnO nanowire (Nw-ZnO) arrays and ZnO porous films have been shown interesting as active layers for selective sensors [3], solar cells [4,5], light emitters in LED [6,7], surfaces with tunable wettability [8] and also as photocatalysts [9]. Regarding all the potentials fields of application mentioned, the correlation between the structure, which is often rather complex, and their functional properties is of utmost importance.

Zinc oxide based micro-/nanostructured hierarchical layers are promising photocatalysts because they combine both a large surface area and a good accessibility of the pollutant to the photoactive surface [10–16]. Compared to particle suspensions, these structures avoid the drawback of the separation and recovery of the photocatalyst from the liquid wastewater after the completion of the degradation process. Therefore, they are easily recyclable and the operation costs are reduced.

In the present paper, the photocatalytic degradation of 4-chlorophenol using UV light has been selected as a model reaction because this reaction has grown on importance in the literature to exceed its original significance as a model of an eco-persistent pollutant [17–21]. It has become a standard for evaluating experimental parameters of photocatalysis. Concerning ZnO as a photocatalyst, this reaction is much less documented in comparison with that on TiO₂ [22,23].

The main goals of the paper are (i) the preparation of hierarchical ZnO layers with well-defined and carefully characterized structure, (ii) a detailed experimental study into their photocatalytic performance in the degradation of 4-chlorophenol and the assessment of

* Corresponding author. Tel.: +420 266053945; fax: +420 286582307.

E-mail addresses: jiri.rathousky@jh-inst.cas.cz (J. Rathousky), thierry.pauporte@chimie-paristech.fr (T. Pauporté).

the effect of structure and texture properties on their photocatalytic performance and (iii) the explanation of the observed kinetics and mechanism of photocatalytic degradation of 4-chlorophenol using theoretical quantum chemical computations of particular participating reactions.

2. Experimental

2.1. Preparation of hierarchical layers of ZnO

The ZnO layers were prepared on F-doped SnO_2 (FTO) coated glass (TEC10, Pilkington). The substrates were carefully cleaned with soap, rinsed with deionized water prior to sonication for 5 min in ethanol and 5 min in acetone. Electrodeposition was carried out in a three-electrode cell. The counter-electrode was a zinc wire and the reference electrode was a saturated calomel electrode (SCE) (with a potential at +0.25 V vs NHE) placed in a separate compartment maintained at room temperature. To ensure a deposition as homogeneous as possible, the substrate was fixed to a rotating electrode and the deposition was performed at a constant rotation speed of 300 rotations per minute (rpm). The electrode surface area corresponding to the geometrical area of the film was 3.1 cm^2 . The deposition bath was prepared with MilliQ quality water ($18.2 \text{ M}\Omega \text{ cm}$) and contained 0.1 M KCl and ZnCl_2 as the supporting salt and zinc precursor, respectively. The bath was bubbled for more than 40 min with molecular oxygen prior to the deposition, the bubbling being maintained upon the deposition process.

The ZnO nanowire arrays were prepared at 85°C using 0.2 mM ZnCl_2 [24]. The applied potential was -1.0 V vs the saturated calomel electrode (SCE). The growth time was fixed at 300 min and the mean wire length was about $5 \mu\text{m}$ (samples Nw-ZnO). In the case of the hierarchical structures, a secondary nanocrystalline film was deposited on the ZnO NWs in similar conditions but the ZnCl_2 concentration was 5 mM and the bath was kept at room temperature (25°C) [25]. The growth time was 10 min for samples coded Nw/nc1-ZnO or 240 min for samples coded Nw/nc2-ZnO. The mesoporous ZnO films (hereafter noted *meso*-ZnO) were prepared at 70°C . The bath contained initially 0.1 M KCl as the supporting electrolyte, 5 mM ZnCl_2 and was saturated with molecular oxygen by an intense bubbling. A thin continuous ZnO layer was first produced on the FTO for 10 min [26]. The mesoporous second layer was then electrodeposited. 50 μM eosin Y (EY) was added in the bath and a potential of -1.0 V vs SCE was applied for 20 min. During this step, EY was co-deposited with ZnO and a compact film made of a mixture of ZnO and EY was synthesized [9,27]. EY acted as a structure directing agent for the pore formation. This component was subsequently removed from the film by soaking in a KOH solution at pH 10.5 overnight in order to release the mesopores in the ZnO layer [28]. The ZnO dense films were prepared at 70°C in a bath containing 0.1 KCl and 5 mM ZnCl_2 saturated with molecular oxygen. A potential of -1.0 V vs SCE was applied during 20 min [26]. After deposition, all the films were carefully rinsed with deionized water and heated at 150°C for 1 h.

2.2. The physico-chemical characterization of hierarchical layers

The sample morphologies were examined with a high resolution Ultra 55 Zeiss FEG scanning electron microscope (SEM) at an acceleration voltage of 10 kV. The transmission electron microscopy imaging was done with a JEOL JEM 2011 200 kV apparatus. The absorbance of the films were calculated from the total transmission and total reflection spectra of the layers measured with a Carry 5000 UV–vis–NIR spectrophotometer equipped with an integrating sphere. The photoluminescence (PL) spectra were measured at 293 K and the continuous wave (CW) PL was excited by the 4th

harmonic (266 nm) line of an YAG:Nd laser and dispersed with a HR250 monochromator (Jobin-Yvon) coupled to an UV-enhanced intensified charge coupled device (ICCD) (Roper). Under pulsed laser excitation, PL spectra were recorded in a pseudo CW mode with a continuous integration of the intensity in 300 ms corresponding to 3 full illumination pulses. The accessible geometric surface area of films with a diameter of 20 mm was determined from the adsorption isotherms of Kr at the boiling point of liquid nitrogen (approx. 77 K) using an ASAP 2010 apparatus (Micromeritics). The molecular area of krypton was taken as 0.21 nm^2 as recommended by the equipment producer. Prior to each adsorption measurement, the samples were outgassed at 150°C overnight.

2.3. Photocatalytic experiments

4-Chlorophenol in water with an initial concentration of $1 \times 10^{-4} \text{ mol L}^{-1}$ was photocatalytically degraded in a quartz cell containing 25 mL of solution. In each photocatalytic experiment, first sample of aqueous solution of 4-chlorophenol was taken before the glass slide with the ZnO film was immersed into it. After 30 min of stirring in dark, second sample was taken. Practically equal concentrations of 4-chlorophenol were determined by HPLC for both samples. Consequently, the measured concentrations of 4-chlorophenol were not influenced by possible adsorption on ZnO films under our experimental conditions. The solution temperature in the vessel was kept at 25°C . Photocatalytic experiments were carried out without bubbling. The top of the liquid in the photoreactor was open to air and the solution was stirred by a magnetic stirrer, consequently, the concentration of dissolved oxygen was constant during the experiment owing to its equilibration with oxygen in the ambient air. A Sylvania Lynx-S 11 W BLB lamp irradiated the film surface with UV light (365 nm) at a low power density of 1 mW cm^{-2} . The irradiated area of the ZnO film was 3.1 cm^2 . For each experiment, eight small aliquots were taken from the solution in the reaction vessel at regular time intervals and analyzed by HPLC [21]. We did not observed any photocorrosion of ZnO films under the used conditions. No Zn^+ and Zn^{2+} ions were detected in the aqueous phase after irradiation.

3. Results and discussion

3.1. Characterization of hierarchical ZnO films

Fig. 1 shows the morphology of the structured films prepared by electrodeposition. Fig. 1a presents a mesoporous film (noted *meso*-ZnO) of about $3\text{--}4 \mu\text{m}$ in thickness. A scheme of its structure is displayed in Fig. 1A. The film consists of large single-crystalline grains, containing a network of interconnected fine pores about 10 nm in diameter. The second structure is an array of self-standing ZnO nanowires shown in Fig. 1b and schematically presented in Fig. 1B. The average length of the wires is $5 \mu\text{m}$. The presence of dense small wires could be observed at the bottom of the bigger ones. Fig. 1c and C display a hierarchical structure made of the wires from Fig. 1b serving as a substrate, whose surface was decorated with a conformal porous layer of nanocrystalline ZnO. The nanocrystalline layer prepared at room temperature perfectly covered the wires. We have shown elsewhere that the secondary ZnO phase is epitaxially grown on the ZnO nanowire backbones [29]. For long deposition times of the nanocrystalline phase, the space between the wires was filled and the nanowires were embedded by the secondary phase (Fig. 1d). A schematic view of the structure is shown in Fig. 1D.

The absorbance spectra of the layers are presented in Fig. 2a. The absorption edge below 400 nm is due to the band-gap absorption of ZnO. All the samples were highly light absorbing in the UV due to

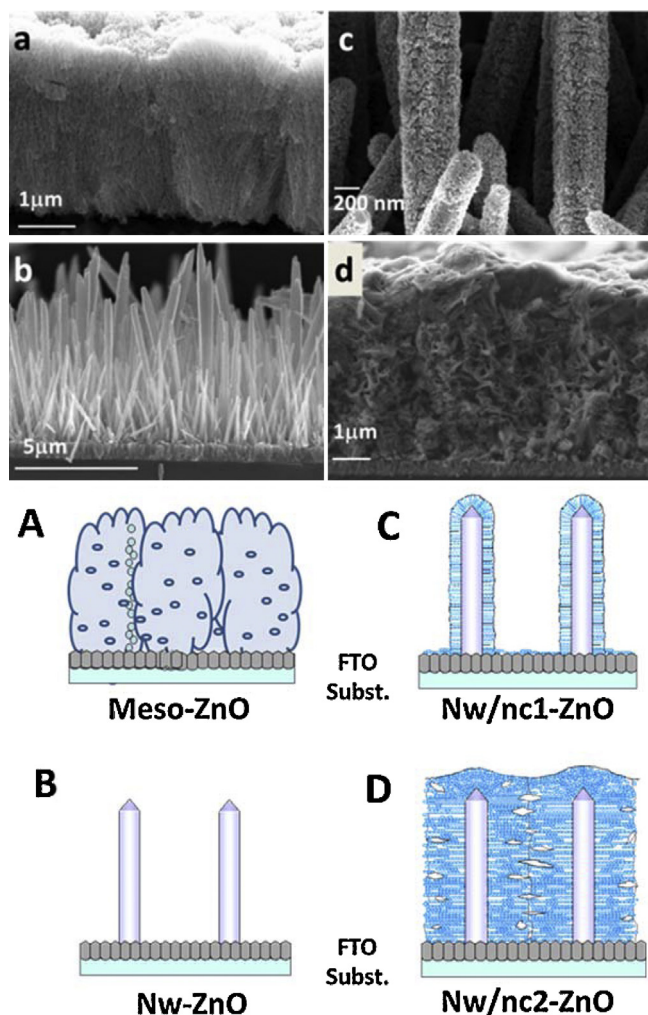


Fig. 1. SEM views (a–d) and schemes (A–D) of the ZnO micro-/nanostructured films. (a and A) mesoporous film (*meso*-ZnO); (b and B) ZnO nanowire arrays (Nw-ZnO); (c and C) ZnO nanowire covered with a thin nanocrystalline ZnO layer (Nw/nc1-ZnO) and (d and D) ZnO nanowire embedded by a thick nanocrystalline ZnO layer (Nw/nc2-ZnO).

their rather high thickness. The inset gives the direct bandgap measurement, E_g , for the various nanostructures. The Nw-based ones had a E_g measured at 3.23 eV, whereas a value of 3.31 eV was found for the mesoporous layer. On the other hand, E_g of the dense film was measured at 3.43 eV. This rather large value can be assigned to the extrinsic *n*-type doping of ZnO by chlorine as described in the reference [26]. The ZnO synthesis is indeed performed in solutions that contain a high concentration of KCl as the supporting salt and chlorine is integrated in the oxide in a more or less extent upon the deposition process. In Fig. 2b, the photoluminescence spectra of the nanostructured films are presented. They were characterized by two emissions, namely a UV excitonic emission due to the radiative near band edge recombination and a broad visible emission peak due to intrinsic deep or surface defects. The Nw-based layers were characterized by a strong UV emission centered at 388 nm. A weak green emission centered at 530 nm was also found. In the literature, the green emission of ZnO has been proposed to originate from oxygen vacancies (V_O), singly ionized oxygen vacancies (V_O^+) [30–32] or surface defects in the case of nanostructures [33,34]. The intensity ratio between the maximum of the two emissions (I_{UV}/I_{vis}) is a good measure of defect states and structural quality of ZnO nanomaterials (see Fig. 2b inset) [26]. The Nw-ZnO sample had the strongest near band edge emission in the UV and a weak emission

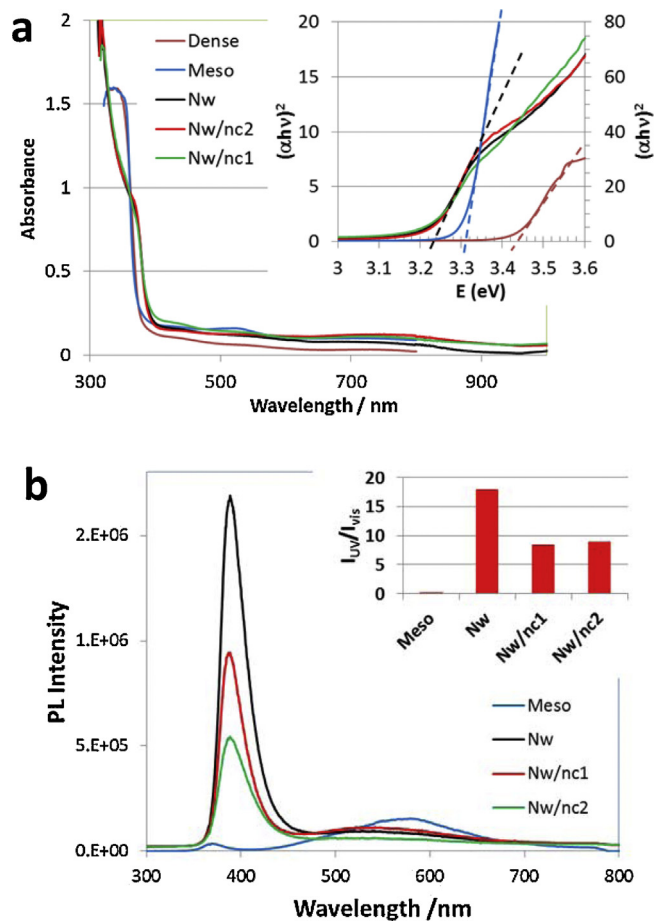


Fig. 2. (a) Absorption spectra of the studied ZnO films. (b) Photoluminescence spectra (inset is the intensity ratios between the maximum of UV and visible photoluminescence). (For interpretation of the references to color in this figure legend, the reader is referred to the web version of this article.)

in the visible range giving an intensity ratio of 18, consequently, the structural quality of this sample was high. The UV emission intensity decreased for the hierarchical structures due to a lower structural quality of the nanocrystalline phase that surrounds the nanowires. For Nw/nc1 and Nw/nc2 samples, the I_{UV}/I_{vis} intensity ratio was measured at 8.9 and 8.4, respectively. The mesoporous ZnO film was less luminescent. The UV emission was centered at 369 nm. The blue shift of this emission can be due to a rather large extrinsic doping of the sample by the chlorine atoms integrated in the lattice structure upon the deposition process (see above) [26]. A strong yellow emission centered at 580 nm was also found combined with a weak green emission. The yellow emission of ZnO is classically assigned to oxygen interstitials defects (O_i) with no surface contribution [34,35]. It is thus, characteristics of the bulk ZnO material. The I_{UV}/I_{vis} intensity ratio was only 0.24 showing a large density of defects in the electrodeposited porous sample.

The texture parameters of the electrodeposited films were investigated by a highly-sensitive Kr adsorption technique. With the exception of Nw-ZnO with a very small surface area ($19 \text{ cm}^2/\text{cm}^2$), the isotherms were characterized by a hysteresis loop (Fig. 3). The adsorption isotherm part at the relative pressure in the range 0.1–0.3 can be very precisely modeled using the BET method, which enables to determine the monolayer capacity and the specific surface area, taking into account the krypton cross-sectional area of 0.21 nm^2 (as suggested by the producer of the adsorption apparatus). The specific surface areas is noted S_{BET} . S_{BET} for *meso*-ZnO and Nw/nc2-ZnO achieved substantial values of

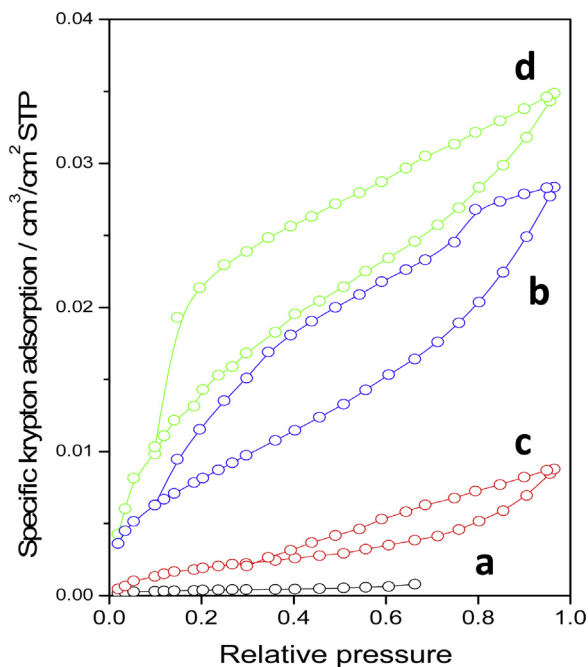


Fig. 3. Kr adsorption isotherms at ca 77 K of the electrodeposited ZnO structured films. (a) Nw-ZnO; (b) meso-ZnO; (c) Nw/nc1-ZnO (Nw-ZnO 5 h + Nc-ZnO 10 min); and Nw/nc2-ZnO (Nw-ZnO 5 h + Nc-ZnO 4 h).

380 and 610 cm²/cm², respectively. The larger S_{BET} for the nw/nc2-ZnO (610 cm²/cm²) compared to nw/nc1-ZnO (98 cm²/cm²) film is partly due to its larger thickness.

The hysteresis loop for the sample Nw/nc1-ZnO is rather narrow, the lower closure point being at the relative pressure of about 0.35. Consequently, this film is characterized by relatively small amount of pores narrower than 10 nm without the presence of very small ones of several nanometers in width. On the contrary, the hysteresis loop for samples meso-ZnO and Nw/nc2-ZnO is very pronounced, covering the range of relative pressure from 0.1 up to 1. Consequently, these samples contain a large amount of pores smaller than about 10 nm including very small pores. As the adsorption isotherm on meso-ZnO, Nw/nc1-ZnO and Nw/nc2-ZnO keep rising at the relative pressure of 1 and do not reach a plateau, all the three samples contain additionally pores larger than 10 nm which are not filled with krypton at ca 77 K.

3.2. Experimental study of the photocatalytic degradation of 4-chlorophenol on structured ZnO films

The photocatalytic activity of structured ZnO films was tested for the degradation, under the UV-light illumination, of 4-chlorophenol, which is an eco-persistent model pollutant [40].

Before the photocatalytic experiments themselves, several blank experiments have been carried out. First a sample film was illuminated in the presence of water for 5 h. Afterwards, the film was removed and 4-chlorophenol was added. In this configuration an experiment analogous to a standard photocatalytic one was carried out, however, without the ZnO film. The outcome was that even if there were some traces of zinc released from the film, their photocatalytic activity in the decomposition of 4-chlorophenol is negligible. This experiment also proved that the direct photolysis of 4-chlorophenol does not occur under the experimental conditions used.

Experimental kinetic data of 4-chlorophenol and 1,4-benzoquinone (BQ) were mathematically treated employing multiple nonlinear curve fitting based on a kinetic model of

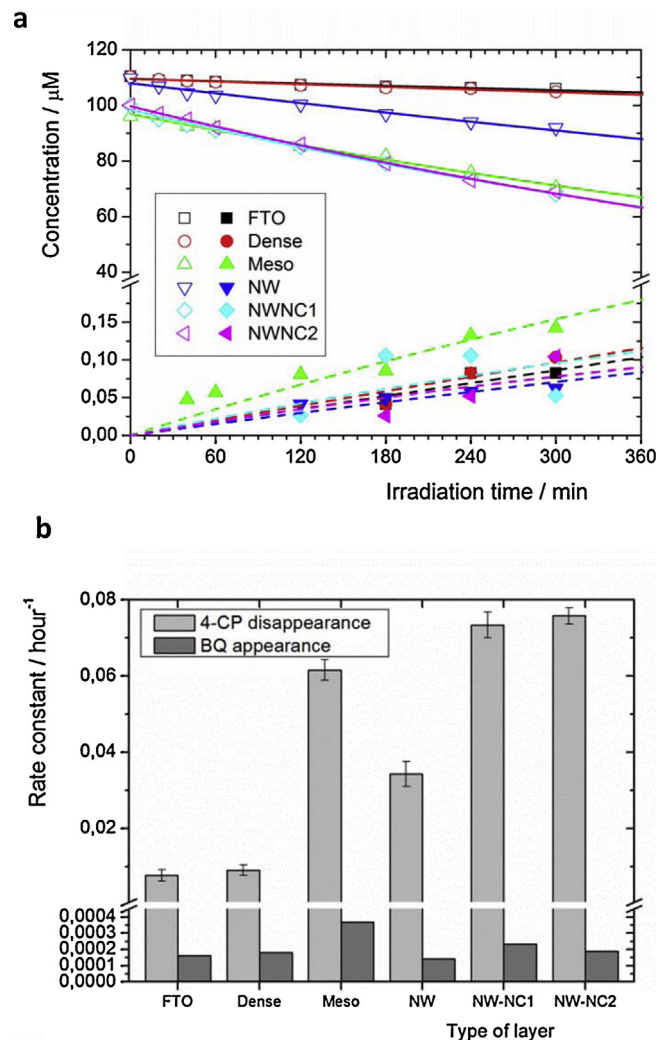


Fig. 4. Photocatalytic degradation of 4-chlorophenol on ZnO films. (a) Time profiles of the starting compound and of a primary intermediate (benzoquinone). FTO film (black solid squares), dense ZnO film (red empty squares), mesoporous film (green solid circles), nanowires Nw (blue empty circles), nanowires with nanocrystals Nw/nc1 (black solid triangles) and Nw/nc2 (red empty triangles). (b) Rate constants of the photocatalytic degradation of 4-chlorophenol and the formation of benzoquinone on ZnO films. (For interpretation of the references to color in this figure legend, the reader is referred to the web version of this article.)

consecutive reactions of the first order $A \rightarrow B \rightarrow C$. Fig. 4a shows the variation of the relative concentration of 4-chlorophenol with illumination time and the appearance of 1,4-benzoquinone (BQ), respectively. The upper fits in Fig. 4a are classical first order decays for A (4-CP) while the bottom fits for the primary product B (BQ) represent typical time profiles of the consecutive reactions of the first order.

Three important conclusions follow from the obtained data. First the rate constants of both reactions, i.e., the 4-chlorophenol disappearance and the BQ appearance are presented in Fig. 4b and clearly depend on the properties of the ZnO photocatalyst. The rate constant for 4-chlorophenol disappearance is the highest for the hierarchical Nw/nc1 and Nw/nc2 samples. Lower disappearance rates are found for meso-ZnO and Nw-ZnO films, whereas the photocatalytic activity of a dense ZnO film is low and similar to that of the bare reference FTO film. The ZnO films have different exposed faces to the aqueous solution: Nw-ZnO and meso-ZnO films have (10–10) exposed facets, [9,36] whereas dense ZnO and the two Nw/nc films (especially Nw/nc1) are preferentially (0001) exposed. In the case of Nw/nc1, Fig. 5 illustrates that this

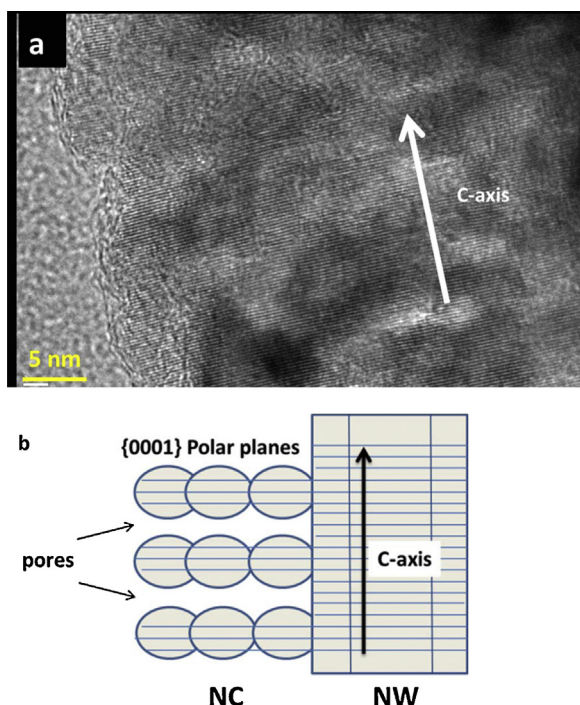


Fig. 5. (a) TEM view and (b) Schematic presentation of the Nw/nc1-ZnO structure. The Nc-ZnO phase is homoepitaxially grown on the *c*-axis oriented Nw-ZnO backbone with pores oriented perpendicular to the wire axis. The pore sidewalls {0001} polar planes exposed.

is due to the homoepitaxial growth of the nanocrystalline phase on the lateral facets of the wire backbone with the pores oriented perpendicular to the wire axis (*c*-axis). The structure with the dominant {0001} family of plane present at the pore sidewalls is schematically shown in Fig. 5b. It is probable that the interaction of 4-chlorophenol is favored on the (0001) polar faces of ZnO which favor the degradation as already observed for organic dyes [12]. Our data also show that a large specific surface area is necessary to achieve a high reaction rate (compare, for example, dense-ZnO and

Nw/nc1 film results). Nw/nc1 and Nw/nc2 films have similar rate constants for 4-chlorophenol disappearance and BQ appearance despite the much larger specific surface area of the latter sample by a factor higher than 6. This shows that the accessibility of the pollutant to ZnO surface is also an important parameter. The Nw/nc1 hierarchical structure is very interesting because it combines both a reasonably high S_{BET} value and a good accessibility of the pollutant to the surface. The rate constant of BQ appearance is low for all the photocatalysts, and is the highest for the *meso*-ZnO sample.

Second the formation of different photocatalytic degradation products of 4-chlorophenol on layers of TiO_2 [17] (for which the main observed intermediate is hydroquinone) and ZnO (benzoquinone) can be explained on the basis of the difference in the point of zero charge (pH_{pzc}). While the width of the band gap and the position of both valence and conducting bands are very similar for both semiconductors, the acido-basic properties of their surface differs substantially. pH_{pzc} of TiO_2 is by about 3 units lower than that of ZnO. Benzoquinone and hydroquinone form a redox couple, whose electrochemical potential equals 0.6992 V vs the NHE. Consequently, the ZnO surface is more positively charged at the conditions of the photocatalytic experiment than that of TiO_2 . Therefore, the photogenerated electrons are more efficiently trapped at the ZnO surface and the electrons on the TiO_2 surface are more reducing and produce more hydroquinone.

Third the optimized values of the corresponding parameters, i.e., rate constants of the degradation of 4-chlorophenol as well as of the formation and disappearance of the particular intermediates, showed a surprising discrepancy. The sum of reaction rates of formation of all the found intermediates represented only about 10% of the reaction rate of 4-chlorophenol degradation. The remaining 90% might correspond to other intermediates that could not be observed by means of HPLC with absorption detector, probably non-aromatic substances after the opening of benzene ring. (Another possibility of the formation of strongly adsorbed or in water non-soluble products was excluded employing an addition of organic solvents to the samples of irradiated reaction mixture.) Moreover, we have reported similar observations using TiO_2 as photocatalyst [21]. This fact is contradictory to the assumption that 4-chlorocatechol and hydroquinone/benzoquinone represent

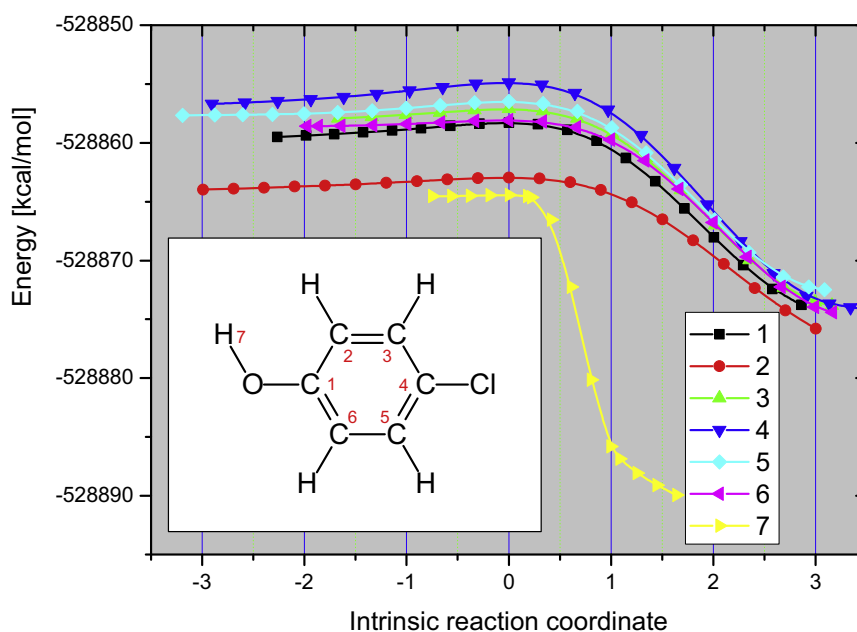


Fig. 6. Reaction coordinates of OH-attacks onto different positions of 4-chlorophenol molecule (indicated by red numbers in the chemical formula). (For interpretation of the references to color in this figure legend, the reader is referred to the web version of this article.)

the only primary intermediates of photocatalytic degradation of 4-chlorophenol [38,39].

There is a evident qualitative correlation between the porosity and photocatalytic activity of the differently prepared ZnO films. However, the insufficient number of the experimental data does not enable any quantitative statistical evaluation.

3.3. DFT modeling of the oxidative degradation of 4-chlorophenol

To explain the above mentioned discrepancy, a detailed theoretical study of an oxidative degradation of 4-chlorophenol was realized. All reaction pathways of an attack of hydroxyl radical (produced by water oxidation) onto various positions of 4-chlorophenol molecule and subsequent reactions with molecular oxygen in its triplet ground state were analyzed employing quantum-chemical calculations by a Gaussian 09W software applying DFT B3LYP/6-31G(d) method. A typical procedure started with the search of transition state connecting the particular reactant and the assumed product. After that the transition structure was found and optimized, a corresponding reaction coordinate

was computed to verify that this transition state really connects the particular starting and final structure. Finally, activation and reaction energies were calculated by comparing zero-point corrected energies of the reactant, product and transition state.

The basis set used in DFT study is 6-31G(d). Additionally we recomputed all OH attacks onto various positions of the molecule of 4-chlorophenol employing the basis set 6-311++G(d). The results are presented and compared with previous computations in supporting information (Fig. S1). However, it can be noted that the use of the higher basis set did not lead to any qualitative changes or new conclusions concerning the investigated reactions. The results of frequency analysis of the transition state are given in the supporting information (Tables S1 and S2).

First, attacks of hydroxyl radical onto all possible positions of the 4-chlorophenol molecule were investigated. The results are graphically shown in the energy diagram of corresponding reaction coordinates in Fig. 6 as well as numerically in the reaction scheme of particular pathways of the OH-attacks with subsequent H-abstractions by triplet oxygen in Fig. 7.

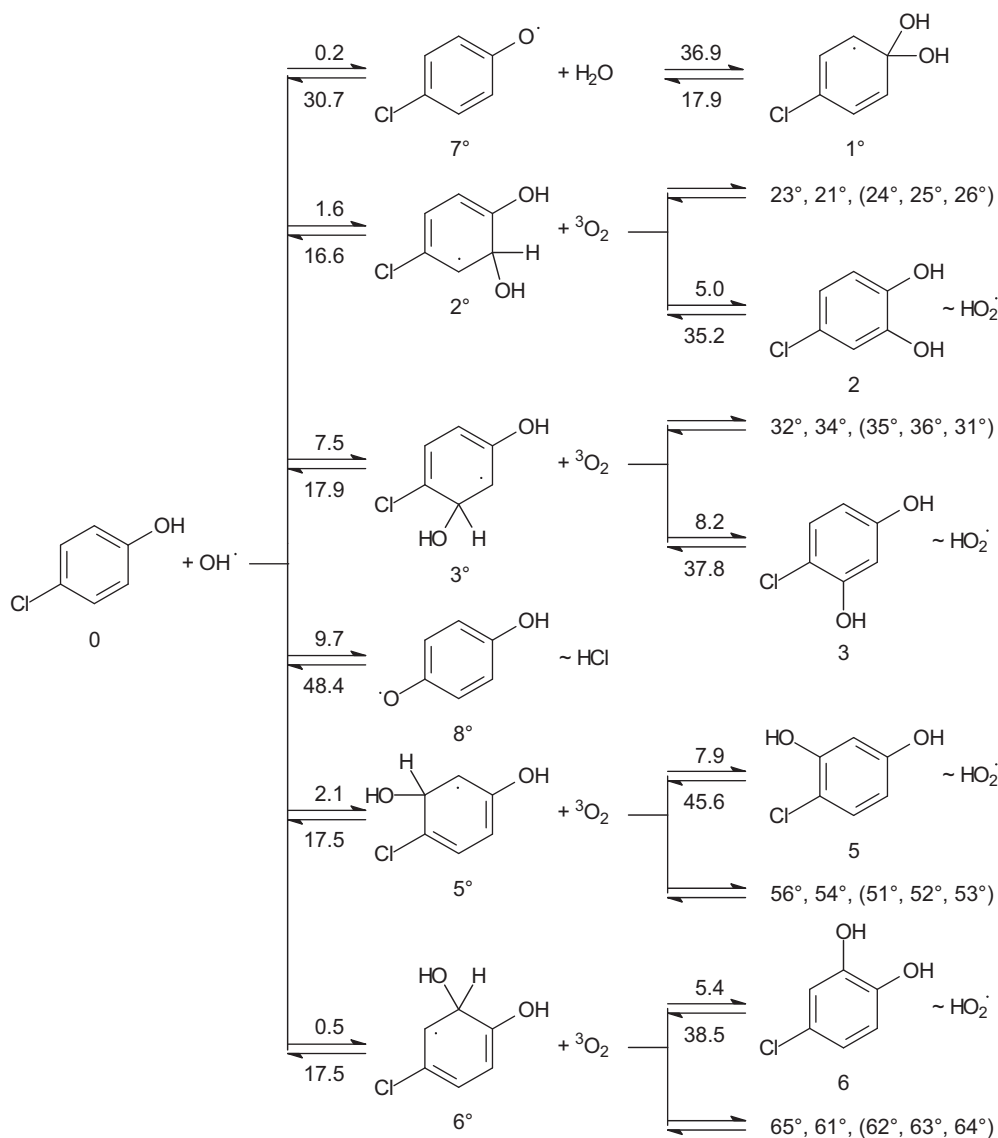


Fig. 7. Reaction scheme of an oxidative degradation of 4-chlorophenol with initial OH-attacks onto various positions of 4-chlorophenol and subsequent H-abstractions by triplet oxygen (numbers at arrows give activation energies in kcal/mol; two-digit numbers XY° indicate subsequent radical transients with —OH and —OO• group in position X and Y, respectively).

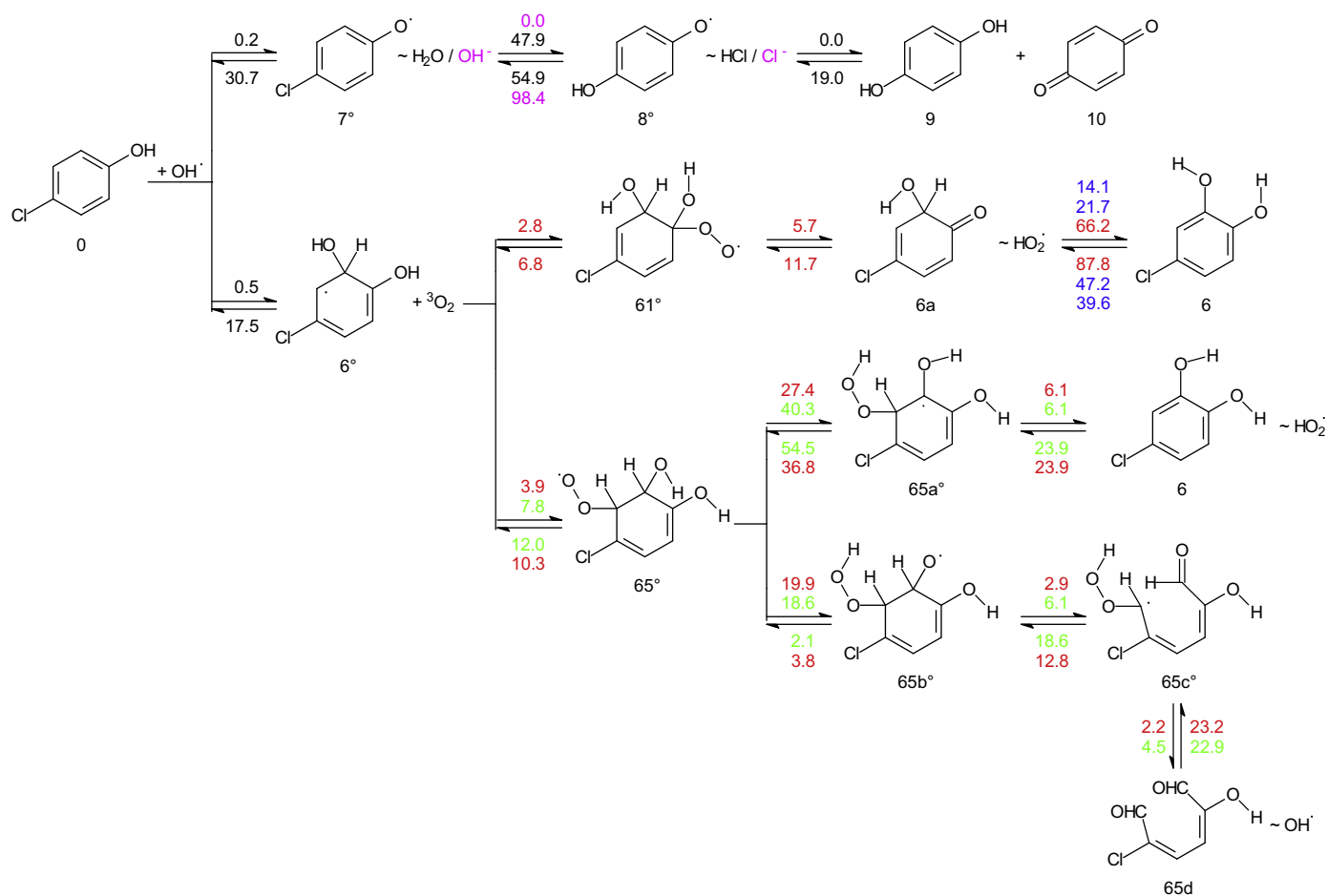


Fig. 8. Typical reaction pathways of an oxidative degradation 4-chlorophenol (0) leading to the identified aromatic products hydroquinone (9), benzoquinone (10) and 4-chlorocatechol (6) as well as to a possible chlorinated ring-opening intermediate (65d) under restoration of OH radical (numbers at arrows give activation energies in kcal/mol, green color corresponds to *cis* while red to *trans* configuration of —OH and —OO^\bullet groups; violet color marks a spontaneous substitution chlorine in position 4 by hydroxyl anion; blue numbers give activation energies of H-transfer reaction mediated by one or two water molecules, respectively). (For interpretation of the references to color in this figure legend, the reader is referred to the web version of this article.)

All primary OH-attacks are strongly exothermic reactions with diffusion-controlled rates (due to very low activation energies between 0.2 and 9.7 kcal/mol). In aerated aqueous solutions containing excess of dissolved molecular oxygen in its ground triplet state, fast exothermic H-abstractions in positions 2,3,5 and 6 follow that lead to 4-chlorocatechol (4-CC) as one of primary stable oxidation products and a less reactive hydroperoxyl radical (HO_2^\bullet).

A direct addition of OH radical onto carbon atom in position 1 cannot be realized because of too close distance from the hydroxyl group in this position. Instead, a preferential abstraction of the hydrogen atom in position 7 proceeds, leading to molecule of water and 4-chlorophenoxyl radical. Comparing energy characteristics (see in Fig. 7), this reaction is the most favorable from all OH-attacks onto 4-chlorophenol molecule. The OH-adduct in position 1 can theoretically result from an addition of water molecule onto 4-chlorophenoxyl radical, which is, however, a slow and endothermic process.

The additions of OH radical into non-substituted 2, 3, 5, and 6 positions should run extremely fast with diffusion-controlled rates (due to their very low activation energies ranging from 0.5 to 7.5 kcal/mol). Also the subsequent abstractions of hydrogen atoms from the same positions by molecular oxygen in its ground triplet state positions are strongly exothermic and should proceed very fast (activation energies from 5.0 to 8.2 kcal/mol). As products, 4-chlorocatechol and 4-chlororesorcinol should be formed.

The last possible OH-attack, onto position 4, should be energetically the less favored (activation energy of 9.7 kcal/mol), however, the most exothermic (activation energy of the reverse reaction is 48.4 kcal/mol). As products, hydrochloric acid and semiquinone radical are created. This radical is also produced by a spontaneous reaction of 4-chlorophenoxyl radical with hydroxyl anion (see in Fig. 8). Semiquinone radicals are known to disproportionate to hydroquinone and benzoquinone that are the other identified primary products of photocatalytic degradation of 4-chlorophenol.

The OH-attacks as well as the subsequent H-abstractions by triplet oxygen should run irreversibly because of the relatively high activation energies of the corresponding reverse reactions (ranged from 16.6 to 48.8 kcal/mol in the case of OH-attacks and from 35.2 to 45.6 kcal/mol for H-abstractions). However, additions of triplet oxygen onto various positions on benzene ring of the primary OH-adducts should proceed very fast and reversibly (activation energies between 3 and 13 kcal/mol in both directions) independently of *cis* or *trans* configuration of —OH and —OO^\bullet groups in the corresponding hydroxy-peroxyl radicals.

The example of typical reaction pathways leading to the observed products (HQ, BQ and CC) as well as to the assumed ring-opening intermediates is shown in Fig. 8. Explicitly noteworthy are parallel intramolecular transformations of hydroxy-peroxyl radicals (with —OH and —OO^\bullet groups in neighboring positions) that should lead either to hydroxylation of the aromatic ring or to its opening under simultaneous restoration of OH radical, which could

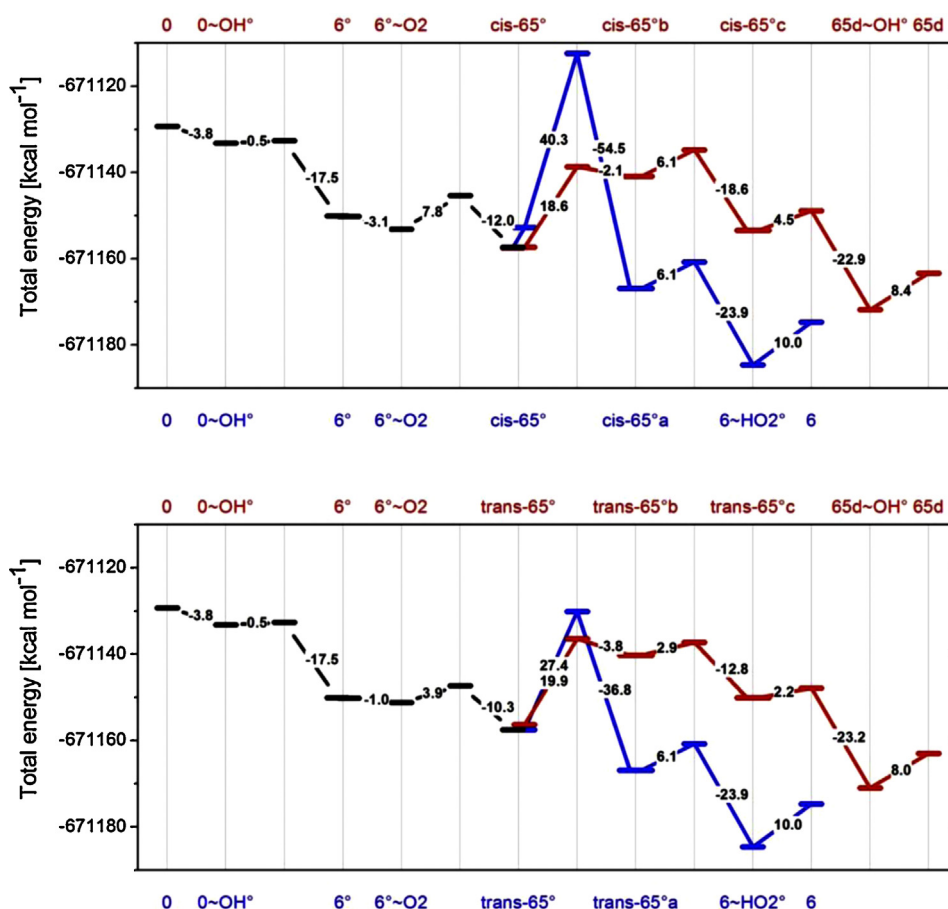


Fig. 9. Energy diagrams of selected pathways of oxidative degradation 4-chlorophenol (0) leading parallel to 4-chlorocatechol (6) and chlorinated ring-opening intermediate (65 d) under simultaneous restoration of OH radical (*cis* (up) and *trans* (down) configuration of —OH and —OO^\bullet groups).

undergo a next OH-attack. Energy diagrams in Fig. 9 give more illustrative views.

The modeling of the degradation of 4-chlorophenol molecules by OH radicals leads to two important conclusions concerning to the interpretation of photocatalytic experiments. First, the hydroxylation of the aromatic ring and its opening occur in parallel. Second, the OH radical can be restored in this mechanism. Therefore, the oxidative degradations of unsaturated organic compounds might proceed more efficiently due to participation of radical chain reactions, as it was shown earlier in the case of the photocatalytic decomposition of oleic acid [37].

4. Conclusions

To sum up, hierarchical ZnO nanoporous/nanowire architectures deposited on a FTO glass substrate have been prepared by a facile two-step electrochemical technique. They strongly absorb UV light and have a high structural quality. The porosity of the hierarchical layers can be tuned by changing the duration of the second growth step. They are environmentally friendly and recyclable photocatalysts for the photodegradation by UV light of 4-chlorophenol, a model compound of an eco-persistent pollutant. The photocatalytic activity of ZnO films is higher than that of an arrayed ZnO nanowire layer and a mesoporous ZnO film. The activity could be enhanced by finely controlling their micro-/nanostructure. The present study shows the importance of developing hierarchical structures with a high percentage exposure of polar (0001) planes, high specific surface area and good accessibility of the pollutant to the oxide surface for achieving high

photocatalytic activity. To interpret the obtained kinetic and mechanistic data of the photocatalytic degradation of 4-chlorophenol, all possible reaction pathways initiated by an attack of hydroxyl radical onto various positions of 4-chlorophenol molecule followed by reactions with triplet oxygen were analyzed in detail employing density functional theory (DFT). The computations have led to several important results, namely that the hydroxylation of the aromatic ring and its opening can occur in parallel releasing hydroperoxyl radical and hydroxyl radical, respectively. The restored OH radical can either further oxidize the primary ring opening product or attack another molecule of 4-chlorophenol. The study provides a new paradigm for further understanding the photocatalytic mechanism on ZnO and suggests new directions to design high-efficiency photocatalytic structures.

Acknowledgements

The authors acknowledge Campus France and the Academy of Science of the Czech Republic for financial support through the PHC Barrande project N° 30987UD. J. Rathousky, R. Zouzelka, H. Bibova-Lipsova and J. Jirkovsky are grateful to the Ministry of Culture of the Czech Republic (grant No. DF11P01OVV012) for the financial support.

Appendix A. Supplementary data

Supplementary data associated with this article can be found, in the online version, at <http://dx.doi.org/10.1016/j.apcatb.2014.12.041>.

References

- [1] U. Ozgur, Y.I. Alivov, C. Liu, A. Teke, M.A. Reshchikov, S. Dogan, V. Avrutin, S.J. Cho, H. Morkoc, *J. Appl. Phys.* 98 (2005) 41301.
- [2] Z.I. Wang, *J. Phys. Condens. Matter* 16 (2004) R829–R858.
- [3] O. Lupan, G. Chai, L. Chow, *Microelectron. J.* 38 (2007) 1211–1216.
- [4] V.M. Guérin, C. Magne, T. Pauporté, T. Le Bahers, J. Rathousky, *ACS Appl. Mater. Interfaces* 2 (2010) 3677–3685.
- [5] V.M. Guérin, T. Pauporté, *Energy Environ. Sci.* 4 (2011) 2971–2979.
- [6] M.C. Jeong, B.Y. Oh, M.H. Ham, S.W. Lee, J.M. Myong, *Small* 3 (2007) 568–572.
- [7] O. Lupan, T. Pauporté, B. Viana, I.M. Tiginyanu, V.V. Ursaki, R. Cortès, *ACS Appl. Mater. Interfaces* 2 (2010) 2083–2090.
- [8] C. Badre, T. Pauporté, *Adv. Mater.* 21 (2009) 697–701.
- [9] T. Pauporté, J. Rathousky, *J. Phys. Chem. C* 111 (2007) 7639–7644.
- [10] Y.H. Zheng, L.R. Zheng, Y.Y. Zhan, X.Y. Lin, Q. Zheng, K.M. Wei, *Inorg. Chem.* 46 (2007) 6980–6986.
- [11] S.S. Ma, R. Li, C.P. Lv, W. Xu, X.L. Gou, *J. Hazard. Mater.* 192 (2011) 730–740.
- [12] S. He, S. Zhang, L. Lu, Y. Zhao, J. Ma, M. Wei, D.G. Evans, X. Duan, *Chem. Commun.* 47 (2011) 1097–10799.
- [13] F. Xu, Y. Shen, L. Sun, H. Zeng, Y. Lu, *Nanoscale* 3 (2011) 5020–5025.
- [14] D. Bekermann, A. Gasparotto, D. Barreca, C. Maccato, M. Rossi, R. Matassa, I. Cianchetta, S. Orlanducci, M. Kete, U. Lavrenic Stangar, *Cryst. Growth Des.* 12 (2012) 5118–5124.
- [15] D. Bekermann, A. Gasparotto, D. Barreca, A. Devi, R.A. Fischer, M. Kete, U. Lavrenic Stangar, O.I. Lebedev, C. Maccato, E. Tondello, G. Van Tendeloo, *ChemPhysChem* 11 (2010) 2337–2340.
- [16] D. Barreca, A. Gasparotto, C. Maccato, E. Tondello, U. Lavrenic Stangar, S.R. Patil, *Surf. Coat. Technol.* 203 (2009) 2041–2045.
- [17] S.S. Shinde, P.S. Shinde, C.H. Bhosale, K.Y. Raipure, J. Photochem. Photobiol. B. Biol. 104 (2011) 425–433.
- [18] G. Alsayyed, J.C. Doliveira, P. Pichat, *J. Photochem. Photobiol. A* 58 (1991) 99–114.
- [19] J. Theurich, M. Lindner, D.W. Bahnemann, *Langmuir* 12 (1996) 6376–6568.
- [20] C. Lettmann, K. Hildenbrand, H. Kisch, W. Macyk, W.F. Maier, *Appl. Catal. B* 32 (2001) 215–227.
- [21] J. Rathousky, V. Kalousek, M. Kolar, J. Jirkovsky, *Photochem. Photobiol. Sci.* 10 (2011) 419–424.
- [22] H.H. Ou, S.L. Lo, C.H. Wu, *J. Hazard. Mater.* 137 (2006) 1362–1370.
- [23] U.I. Gaya, A. Abdullah, Z. Zainal, M.Z. Hussein, *J. Hazard. Mater.* 168 (2009) 57–63.
- [24] T. Pauporté, G. Bataille, L. Joulaud, F.J. Vermersch, *J. Phys. Chem. C* 114 (2010) 194–202.
- [25] T. Pauporté, I. Jirka, *Electrochim. Acta* 54 (2009) 7558–7564.
- [26] T. Pauporté, E. Jouanno, F. Pellé, B. Viana, P. Aschehoug, *J. Phys. Chem. C* 113 (2009) 10422–10431.
- [27] T. Pauporté, T. Yoshida, A. Goux, D. Lincot, *J. Electroanal. Chem.* 534 (2002) 55–64.
- [28] T. Yoshida, M. Iwaya, H. Ando, T. Oekermann, K. Nonomura, D. Schlottwein, D. Wöhrle, H. Minura, *Chem. Commun.* 4 (2004) 400–401.
- [29] V.M. Guérin, J. Rathousky, T. Pauporté, *Sol. Energy Mater. Sol. Cells* 102 (2012) 8–14.
- [30] M. Izaki, M. Watase, H. Takahashi, *Adv. Mater.* 15 (2003) 2000–2002.
- [31] Y. Chen, D.M. Bagnall, H.J. Koh, K.T. Park, K. Hiraga, Z. Zhu, T. Yao, *J. Appl. Phys.* 84 (1998) 3912–3918.
- [32] C.H. Ahn, Y.Y. Kim, D.C. Kim, S.K. Mohanta, H.K. Cho, *J. Appl. Phys.* 105 (2009) 013502.
- [33] B.X.Z.X. Liu Fu, Y.B. Jia, *Appl. Phys. Lett.* 79 (2001) 943–945.
- [34] D. Li, Y.H. Leung, A.B. Djuricic, Z.T. Liu, M.H. Xie, S.L. Shi, S.J. Xu, W.K. Chan, *Appl. Phys. Lett.* 85 (2004) 1601–1603.
- [35] M. Liu, A.H. Kitai, P. Mascher, *J. Lumin.* 54 (1992) 35–42.
- [36] H. El Belghiti, T. Pauporte, D. Lincot, *Phys. Status Solidi (a)* 205 (2008) 2360–2364.
- [37] J. Rathousky, V. Kalousek, M. Kolar, J. Jirkovsky, P. Bartak, *Catal. Today* 161 (2011) 202–208.
- [38] X. Li, J.W. Cubbage, T.A. Tetzlaff, W.S. Jenks, *J. Org. Chem.* 64 (1999) 8509–8524.
- [39] X. Li, J.W. Cubbage, W.S. Jenks, *J. Org. Chem.* 64 (1999) 8525–8536.
- [40] P.K.J. Robertson, D.W. Bahnemann, J.M.C. Robertson, F. Wood, In: *Photocatalytic Detoxification Of Water and Air-Hdb. Env. Chem. Vol. 2, Part M*, Springer-Verlag, Berlin, Heidelberg, 2005, pp. 367–423.